Available online at www.sciencedirect.com
SCIENCE DIRECT®
Journal of Magnetic Resonance 168 (2004) 103–109
JMR Journal of Magnetic Resonance
www.elsevier.com/locate/jmr

Design of a constant adiabaticity pulse for selective population inversion

Lorenz Mitschang,* Bernd Ittermann, Florian Schubert, and Herbert Rinneberg

Physikalisch-Technische Bundesanstalt, Division of Medical Physics and Metrological Information Technology, Abbestr. 2–12, 10587 Berlin, Germany

Received 2 October 2003; revised 28 January 2004

Abstract

A new adiabatic pulse for population inversion and the principles of its design are presented. The pulse shape is characterized by the combination of two constraints. (i) Adiabatic following of the central isochromat of the spectral region of interest occurs with constant, possibly small adiabaticity parameter; thereby, the center isochromat gets most efficiently inverted. (ii) Frequency and amplitude modulations obey the principle of offset-independent adiabaticity; thus, the inversion dynamics of the center isochromat is extended over the desired bandwidth. Selective population inversion can be achieved rather independently of spatial radio frequency field inhomogeneities and with significantly reduced peak RF amplitude in comparison with the well-known sech/tanh adiabatic pulse.

Keywords: RF pulse design; Adiabatic pulse; Selective inversion; RF peak amplitude

1. Introduction

Adiabatic following is a versatile experimental technique to manipulate spin ensembles since it is rather insensitive to fluctuations in dynamical and experimental parameters. In comparison with conventional pulse techniques in high-resolution NMR, polarization, and coherence transfer can be enhanced [1–3], and broadband spin decoupling can be achieved with reduced field amplitude [4,5]. Adiabatic following is very efficient for the inversion of nuclear spins over a specified range of transition frequencies, even when subjected to a spatially inhomogeneous radio frequency (RF) field [6]. Such conditions arise in many practical situation, e.g., when surface coils are used whose RF amplitude declines strongly with distance from the coil center. The performance of adiabatic following, however, depends crucially on the specific choice of amplitude and frequency modulations of the RF field. Principally, any modulation scheme can induce adiabatic following as long as it is slowed down sufficiently for the adiabatic approximation to be valid [7]. In practice, however, limitations exist for the execution time because relaxation losses occur concomitantly, for the absorbed pulse energy because sample heating can be a hazard, particularly in human applications, and for the peak RF amplitude because high power loads can provoke probe arcing. In addition, spectral selectivity of adiabatic following is pivotal in many applications, e.g., for the slice selective approach in magnetic resonance imaging (MRI).

To serve the practical needs as good as possible, a number of modulation schemes have been specifically designed [5,6]. The difficulty is to satisfy the adiabatic approximation within an ensemble optimally. For an individual isochromat, on the other hand, it is a simple matter to do: adiabatic following is most efficient when performed throughout at the threshold of validity of the adiabatic approximation [7]. This approach was employed for the construction of the constant adiabaticity pulse [8]. It is not widely in use anymore for broadband inversion, since its selectivity is limited and high power is required. We present the extension of the constant adiabaticity principle for the design of an efficient selective broadband inversion pulse. The performance of the new

* Corresponding author. Fax: +49-30-3481505.
E-mail address: Lorenz.Mitschang@ptb.de (L. Mitschang).

1090-7807/$ - see front matter © 2004 Elsevier Inc. All rights reserved.
doi:10.1016/j.jmr.2004.02.003

pulse is compared with that of the well-known sech/tanh adiabatic pulse [9].

2. Constant adiabaticity pulses

We consider an individual spin−1/2, the center isochromat, with transition frequency ω_0 in a Zeeman field subjected to a circularly polarized RF field of time-dependent carrier frequency $\omega(t)$ and amplitude $\omega_1(t)$. In a frame of reference rotating at any instant with frequency $\omega(t)$ around the Zeeman field and having its $-x$-axis aligned along the RF field (frequency frame), the resonance offset $\Delta(t) = \omega_0 - \omega(t)$ and field amplitude determine the length $\omega_{\text{eff}}(t) = \sqrt{\Delta(t)^2 + \omega_1(t)^2}$ and polar angle $\theta(t) = \arccos(-\Delta(t)/\omega_{\text{eff}}(t))$ of the effective field. The center isochromat obeys adiabatic following, i.e., follows the reorienting effective field, as long as the adiabatic condition is valid [7]. It can be conveniently expressed in terms of the adiabaticity parameter $k(\omega_0, t) = |\omega_{\text{eff}}(t)/\dot{\theta}(t)|$ as $k(\omega_0, t) \gg 1$, where the dot indicates derivative with respect to time. As the adiabaticity parameter approaches unity, the more rapidly the effective field reorients but the isochromat ever stronger fails to follow it properly. We can define a threshold value k_0 below which the adiabaticity parameter should not drop to assure adiabatic following of sufficient quality for the purpose in question. Thus, adiabatic following of the center isochromat is achieved most efficiently, if the adiabatic condition is fulfilled with that smallest yet tolerable threshold value throughout the complete process. The modulations $\Delta(t)$ and $\omega_1(t)$ then satisfy the expression

$$\dot{\theta}(t) = \omega_{\text{eff}}(t)/k_0. \tag{1}$$

Many different pairs of functions may resolve Eq. (1), and may induce—besides efficient adiabatic following of the center isochromat—a caleidoscope of spin manipulations at transition frequencies different from ω_0. For the constant adiabaticity pulse, Eq. (1) was solved under the assumption of a constant RF field amplitude [8]. Since the frequency sweep extends to infinity in this case, any isochromat—irrespective of its transition frequency—is affected by the pulse, hampering spectral selectivity. This also implies an uneconomical spectral distribution of the pulse energy. To identify those modulation schemes which obey the principle of constant adiabaticity and enable efficient selective inversion at the same time, a suitable condition, different from constancy of the field amplitude, must be posed. The principle of offset-independent adiabaticity [10,11] relates frequency and amplitude modulations by

$$\dot{\Delta}(t) = \omega_1(t)^2/K. \tag{2}$$

A flat inversion profile over a specified range of transition frequencies is enforced by an equal distribution of the pulse energy [11]. Whenever the frequency sweep traverses a resonance, the adiabaticity parameter referring to the corresponding isochromat within the specified bandwidth adopts the very same constant value K. For the center isochromat, clearly $K = k_0$ holds if the adiabaticity parameter is constrained to be constant. Thus, Eqs. (1) and (2) can be combined in case of the center isochromat to a differential equation defining the pulse shape

$$\ddot{\theta}(t) = \dot{\theta}(t)^2 \tan\theta(t)(1 - \sin\theta(t)). \tag{3}$$

For proper inversion of the center isochromat, $\theta(t)$ should increase monotonically from 0, where the effective field points along the frequency frame z-axis, to π, where it points along the $-z$-axis, during the pulse. Thus, the polar angle θ can be used instead of time t as the independent variable to describe the pulse shape. Eq. (3) becomes the separable form

$$\dot{\theta}(\theta)' = \dot{\theta}(\theta)\tan\theta(1 - \sin\theta), \tag{4}$$

where the prime denotes the derivative with respect to θ. It is by no means obvious that Eq. (4) generates viable pulse shapes. The expression $\tan\theta(1 - \sin\theta)$ on the right hand side is well-behaved for all $\theta \in [0, \pi]$. Therefore, any finite value can be chosen for the initial angular velocity $\dot{\theta}(0) = \omega_{\text{eff}}(0)/k_0 = \sigma/k_0$. The positive constant σ is also the negative of the initial value of the frequency sweep, because we require $\theta(0) = 0$. For a proper pulse shape it should have the meaning of the lower boundary point of the inversion band which is the case if no smaller values than $-\sigma$ are hit by the frequency sweep. With the transformations $\Delta(\theta) = -\omega_{\text{eff}}(\theta)\cos\theta$ and $\omega_1(\theta) = \omega_{\text{eff}}(\theta)\sin\theta$ and the relation $\omega_{\text{eff}}(\theta)'/\omega_{\text{eff}}(\theta) = \dot{\theta}(\theta)'/\dot{\theta}(\theta)$ from Eq. (1) we obtain the derivative

$$\frac{\mathrm{d}\Delta}{\mathrm{d}\omega_1} = \frac{\Delta'/\omega_{\text{eff}}}{\omega_1'/\omega_{\text{eff}}} = \frac{-\tan\theta(1 - \sin\theta)\cos\theta + \sin\theta}{\tan\theta(1 - \sin\theta)\sin\theta + \cos\theta}, \tag{5}$$

for a half passage ($\theta \in [0, \pi/2]$). It is zero for $\theta = 0$, increases monotonically with increasing RF amplitude, and approaches a positive singularity at $\theta = \pi/2$. Similarly, in the second half passage ($\theta \in [\pi/2, \pi]$), the frequency sweep further increases monotonically, this time with decreasing RF amplitude, until it levels off at σ. Thus, the inversion bandwidth is just given by 2σ.

Elementary integration of Eq. (4) provides $\dot{\theta}(\theta)$ and from Eq. (1) we get

$$\omega_{\text{eff}}(\theta) = \sigma\frac{\exp\{\sin\theta\}}{\cos\theta\tan\left(\frac{\pi}{4} + \frac{\theta}{2}\right)}, \quad \theta \in [0, \pi]. \tag{6}$$

The analytic solution in Eq. (6), the pulse shape in polar coordinates with the polar angle as the independent variable, is just the trajectory of the effective field in frequency frame. The rate of motion upon the trajectory is $\dot{\theta}(\theta) = \omega_{\text{eff}}(\theta)/k_0$. The frequency and amplitude

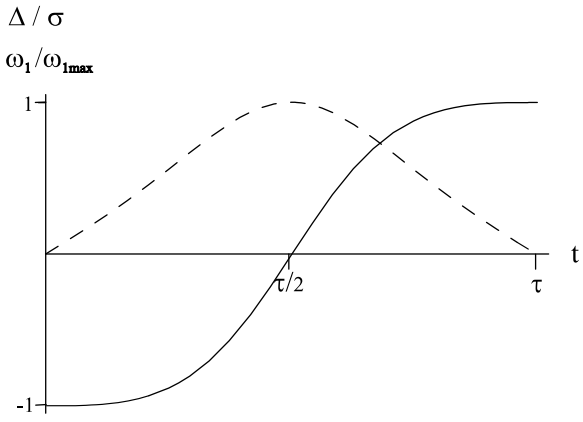

Fig. 1. Pulse shape of the new adiabatic pulse. Normalized amplitude (dashed) and frequency (solid) modulations as functions of time [12].

modulations as functions of the polar angle are readily deduced from Eq. (6). Their more conventional form as functions of time requires knowledge of the inverse function of $t = \int_0^\theta \mathrm{d}\theta/\dot{\theta}(\theta)$ which we were only able to obtain numerically. The normalized modulation functions are displayed in Fig. 1 [12]. Again by numerical integration, the pulse length is obtained as

$$\tau = \int_0^\pi \mathrm{d}\theta/\dot{\theta}(\theta) = 2.683\frac{k_0}{\sigma} = 3.647\frac{k_0}{\omega_{1\,\max}}, \qquad (7)$$

where $\omega_{1\,\max}$ is the peak RF amplitude of the pulse which obeys $\omega_{1\,\max}/\sigma = e/2$ from Eq. (6). Finally, the area of an inverting pulse is given by

$$A = \int_0^\tau \omega_1(t)\,\mathrm{d}t = \int_0^\pi \omega_1(\theta)\,\mathrm{d}\theta/\dot{\theta}(\theta) = 2k_0. \qquad (8)$$

The original constant adiabaticity pulse under the constraint of a constant pulse amplitude has pulse length $2k_0/\omega_1$ and area $2k_0$ for inversion [8]. Thus, in comparison offset-independent adiabaticity enforces adiabaticity over a well-defined bandwidth by slowing down the pulse for given peak amplitude and adiabaticity parameter while the pulse area is preserved.

3. Comparison with sech/tanh pulse

Adiabatic following implies tolerance to parameter variation over the considered ensemble which we assess through simulated and experimental inversion profiles by comparison with the well-known sech/tanh adiabatic pulse (amplitude modulation sech(x), frequency modulation tanh(x)) [9]. The sech/tanh pulse is much appreciated, particularly in MRI, for its high selectivity which is due to the peaked nature of the sech amplitude modulation [11]. In our comparison, the pulses are tuned to a bandwidth of 8 kHz (the center isochromat is at the center of the band) and a pulse length of 9 ms, typical specifications for slice-selection in MRI.

Table 1
Ratio of simulated pulse performance parameters for 9 ms pulse length and 8 kHz bandwidth

$\frac{\omega_{1\,\max}(\mathrm{HS})}{\omega_{1\,\max}(\mathrm{CA})}$	$\frac{E(\mathrm{HS})}{E(\mathrm{CA})}$	$\frac{\omega_1^{95\%}(\mathrm{HS})}{\omega_1^{95\%}(\mathrm{CA})}$	$\frac{\delta_{95\%}(\mathrm{HS})}{\delta_{95\%}(\mathrm{CA})}$	$\frac{\delta_{2500\,\mathrm{Hz}}(\mathrm{HS})}{\delta_{2500\,\mathrm{Hz}}(\mathrm{CA})}$
1.45	0.99	1.39	1.10	0.45

Abbreviations and definitions: HS, sech/tanh pulse; CA, new constant adiabaticity pulse; $\omega_{1\,\max}$, peak RF amplitude to achieve a specified inversion efficiency of the center isochromat; E, pulse energy; $\omega_1^{95\%}$, peak RF amplitude to achieve 95% inversion efficiency homogeneously throughout the specified bandwidth ($\omega_1^{95\%}/2\pi = 1206$ and 868 Hz for the sech/tanh pulse and the new pulse, respectively); $\delta_{95\%}$, width of transition region at peak RF amplitude $\omega_1^{95\%}$; $\delta_{2500\,\mathrm{Hz}}$, width of transition region at peak RF amplitude of 2500 Hz. The width of transition region (see Fig. 2) is defined as the range of transition frequencies with inversion efficiency between 95% (in-slice) and 5% (out-of-slice).

The corresponding parameter settings for the new pulse are $\sigma = 4\,\mathrm{kHz}$ and $k_0 = 84$. In case of the sech/tanh pulse the parameters in the original symbolism of Silver et al. [9] become $\beta = 1178\,\mathrm{kHz}$ and $\mu = 3.4$ for a pulse amplitude truncated at 1% of its maximum. The quantitative comparison of the performance of both pulses is summarized in Table 1.

In the simulations, the z-component of magnetization M_z at the end of the pulse is calculated by numerical solution of the Bloch equation ignoring relaxation and assuming thermal equilibrium magnetization M_0 initially [13]. The efficiency of population inversion is measured in percentage according to $\frac{1}{2}(1 - M_z/M_0) \times 100\%$.

For the experiments, the sech/tanh pulse and the new adiabatic pulse, both tuned for inversion of a 8 kHz bandwidth and to a length of 9 ms, were implemented on a 3 T whole body scanner (MEDSPEC 30/100, Bruker Medical). The adiabatic pulses were applied in the presence of a Zeeman field gradient and after 6.5 ms a subsequent spin-echo sequence with echo time 160 ms was used to image the slice profiles. The phantom was a cylinder of 24-cm length and 14-cm in diameter, placed within the head coil of the system with its axis along the Zeeman gradient direction. The cylinder was filled with agarose gel containing 1.33 g/L NaCl and doped with 0.67 g/L $CuSO_4$ to establish a proton longitudinal relaxation time of about 800 ms. Changes less than ± 0.2 dB in the peak RF amplitude could barely manifest in an observable modification of a slice profile. Thus, the relative error in the peak RF amplitude determination is estimated to be <2.4%. The linewidth of the proton signal of the phantom was 6 Hz which generates only a minor broadening in the experimental profiles in comparison with the simulated ones which are just M_z/M_0 at the end of a pulse. All slice profiles are presented in magnitude mode which allows for an easy estimation of the performance.

Adiabaticity is best demonstrated by the insensitivity of broadband inversion to spatial RF field inhomogeneity. In Fig. 2, simulated contour plots of M_z/M_0 at the

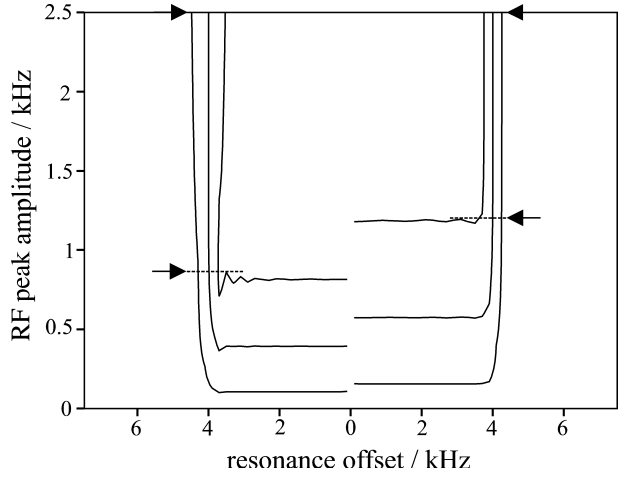

Fig. 2. Performance of population inversion. Contours of calculated normalized longitudinal magnetization M_z/M_0 at the end of the new adiabatic pulse (LHS) and the sech/tanh pulse (RHS) in dependence of resonance offset to the center isochromat and the peak RF amplitude. Both pulses are set up for an inversion bandwidth of 8 kHz and a length of 9 ms. The inner, middle, and outer line indicate 95, 50, and 5% inversion efficiency, respectively. The arrows indicate positions (peak RF amplitude) for comparison of the width of the transition region in Table 1.

end of a pulse are displayed in dependence of resonance offset to the center isochromat and peak RF amplitude. Both pulses achieve inversion homogeneously over the specified bandwidth. The slice profile is retained, even for large variations in the peak RF amplitude. The sech/tanh pulse, however, always requires a 45% higher peak RF amplitude than the new pulse if the same inversion efficiency with respect to the center isochromat must be obtained (e.g., 95, 50, or 5%; see contours in Fig. 2).

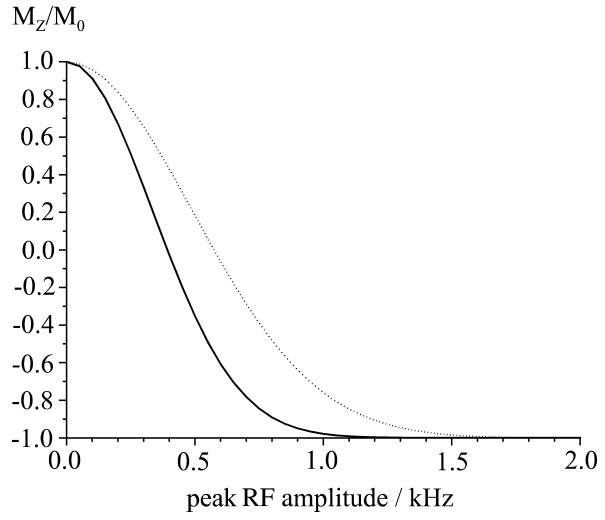

Fig. 3. Adiabaticity of spin inversion. Calculated normalized longitudinal magnetization of the center isochromat at the end of the new adiabatic pulse (solid) and the sech/tanh pulse (dotted) in dependence of the peak RF amplitude.

Thus, the peak power to be generated by the RF amplifier and to be transmitted by the RF coil for a sech/tanh pulse is more than twofold that of the new pulse. This point is further demonstrated in Fig. 3 which shows an intersection of Fig. 2 with M_z/M_0 at the end of the pulse in dependence of the peak RF amplitude for the center isochromat. Fig. 4 displays simulated and experimental slice profiles when both pulses are applied with an identical peak RF amplitude of 1064 Hz. In contrast to the new pulse, full inversion is not achieved by the sech/tanh pulse. Despite, the large difference in peak RF amplitude for the achievement of proper inversion, however, the energies of both pulses are almost

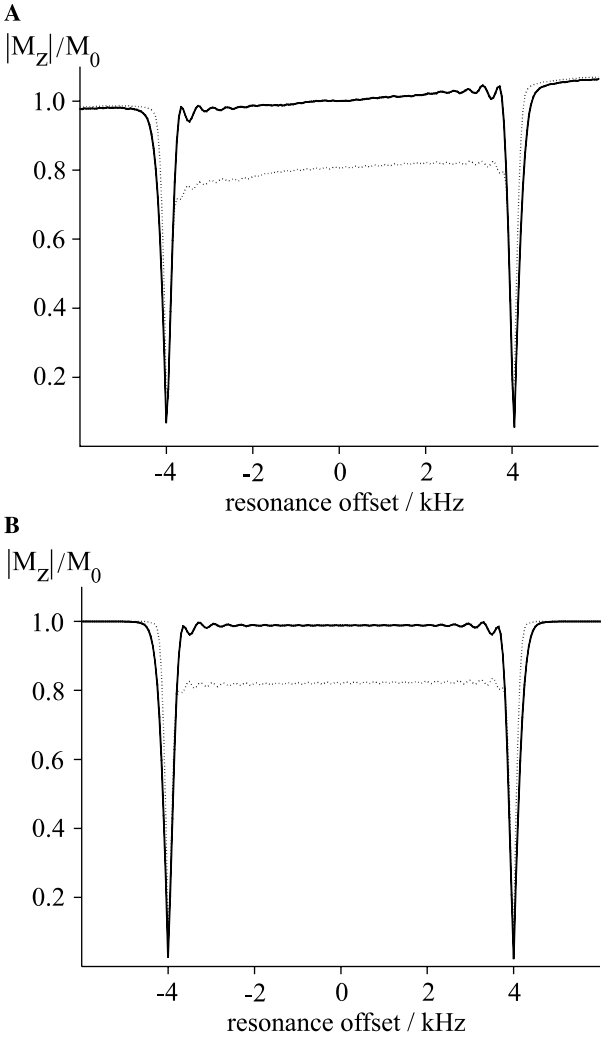

Fig. 4. Comparison of slice profiles. (A) Experimental slice profiles in magnitude representation of the new adiabatic pulse (solid) and the sech/tanh pulse (dotted). Both pulses are set up for an inversion bandwidth of 8 kHz, have a length of 9 ms, and have an identical peak RF amplitude of 1064 Hz. The weak intensity increase in direction of positive resonance offset is caused by an air meniscus on top of the agarose gel within the phantom. (B) The same pulse parameter settings are used to obtain simulated slice profiles for the new adiabatic pulse (solid) and the sech/tanh pulse (dotted).

equal, because the pulse area of the new pulse is larger than for a sech amplitude modulation.

For the new pulse the transition region inverted/non-inverted magnetization increases modestly with the applied peak RF amplitude, whereas in case of the sech/tanh pulse a very sharp transition prevails almost independently of the applied peak RF amplitude. Just at the peak RF amplitude threshold value for 95% homogeneous inversion throughout the bandwidth (see markings in Fig. 2), the new adiabatic pulse apparently generates an even narrower transition region than the sech/tanh pulse. The details are visible in Fig. 5.

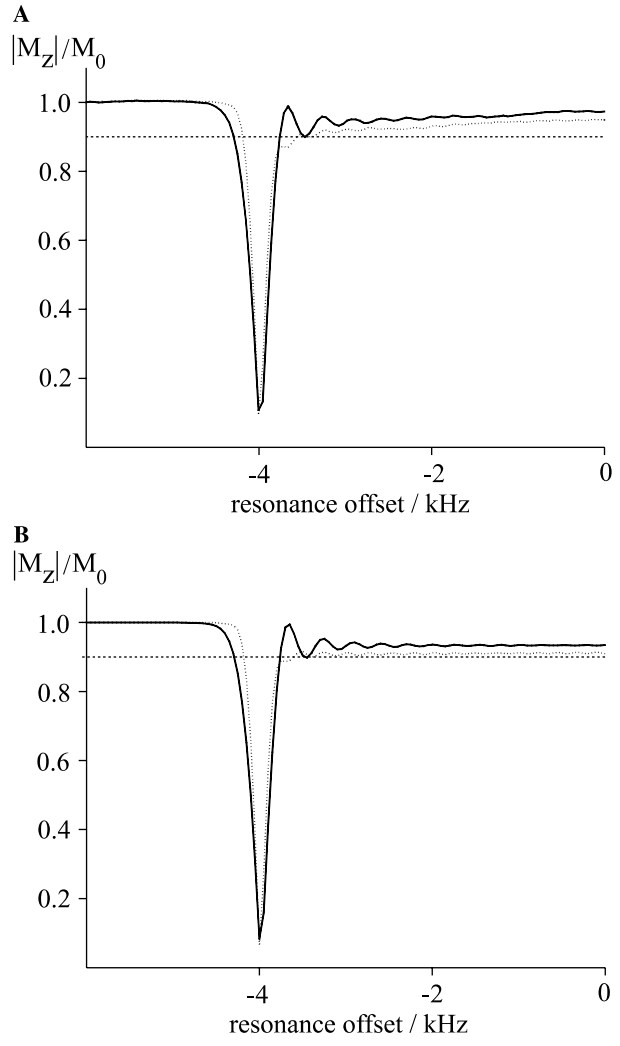

Fig. 5. Width of the transition region inverted/non-inverted magnetization. (A) Cut-outs of experimental slice profiles in magnitude representation of the new adiabatic pulse with peak RF amplitude 868 Hz (solid) and of the sech/tanh pulse with peak RF amplitude 1206 Hz (dotted). The pulses are tuned to a bandwidth of 8 kHz and a length of 9 ms. The weak intensity increase in direction of positive resonance offset is caused by an air meniscus on top of the agarose gel within the phantom. (B) The same pulse parameter settings are used to obtain simulated slice profiles for the new adiabatic pulse (solid) and the sech/tanh pulse (dotted). In (A) and (B), the in-slice and out-of-slice inversion efficiency is at least 95% and at most 5%, respectively, as marked by the parallel to the abscissa (dashed).

Presented are cut-outs of simulated and experimental slice profiles for the new pulse with peak RF amplitude 868 Hz and for the sech/tanh pulse with peak RF amplitude 1206 Hz. The width of the transition region may be specified as the range of transition frequencies where the inversion efficiency is between two, somewhat arbitrarily set, limiting values; they mark within the specified bandwidth (in-slice) proper population inversion and at larger resonance offsets (out-of-slice) the return of magnetization to the equilibrium state, respectively. The dashed parallel to the abscissa in Fig. 5 indicates 95 and 5% inversion efficiency in-slice and out-of-slice, respectively. For that measure, the sech/tanh has a 10% larger transition width in comparison with the new pulse. For other limits, the transition-width ratio for both pulses is different, because the slice profiles change slightly. We found by simulation that the new pulse has a transition width at most equal to that of the sech/tanh pulse for up to 98 and 2% in-slice and out-of-slice inversion efficiency, respectively. At higher and smaller efficiency for in-slice and out-of-slice inversion, respectively, the sech/tanh generates a sharper profile when applied at the appropriate threshold value of the peak RF amplitude.

In summary, at least for negligible spatial inhomogeneity of the RF amplitude the new pulse can achieve selective population inversion at significantly reduced RF field amplitude in comparison with the sech/tanh pulse without increasing energy deposition in the medium or scarifying sharpness of the profile.

4. Discussion

The difference in performance of the new pulse and the sech/tanh pulse must correspond to differences in the basic principles governing the respective pulse shape. But, as is easy to verify, the sech/tanh modulation functions obey offset-independent adiabaticity just like the newly derived shape (see Eq. (2)). An additional property, however, is needed in order to determine the pulse shape uniquely. The elliptic path traversed by the effective field vector during the sech/tanh pulse from the north pole to the south pole of the Bloch sphere in frequency frame may be chosen for this purpose. In case of the new pulse, constancy of the adiabaticity parameter with respect to the center isochromat is used to that end (see Eq. (1)). The resulting trajectory of the effective field vector (Eq. (6)) differs subtle from a perfect elliptic path, as shown in Fig. 6. Thus, the new pulse may be viewed as a modification of the sech/tanh pulse achieved by easing the restriction to an elliptic pulse trajectory, while still satisfying offset-independent adiabaticity. The latter constraint clearly causes the high selectivity of both pulses, for offset-independent adiabaticity ensures a uniform (minimal) adiabaticity parameter over a specified range of transition frequencies for those points in

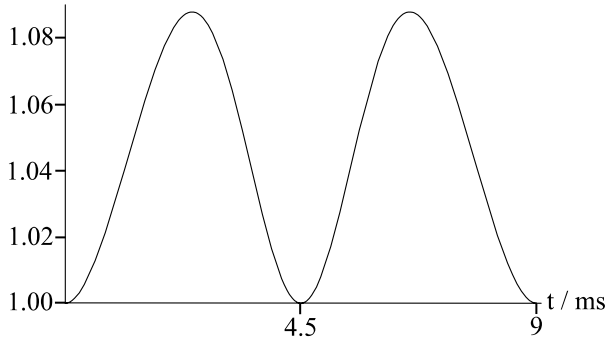

Fig. 6. Deviation of the pulse trajectory of the new adiabatic pulse from an elliptical path. The quantity $(\Delta(t)/\sigma)^2 + (\omega_1(t)/\omega_{1\,\max})^2$ from the modulation functions in Fig. 1 is shown in dependence of the pulse duration for a total pulse length of 9 ms.

time when the frequency sweep hits a resonance [10,11]. The prominent insensitivity to peak RF amplitude variations is not explicitly accounted for in the pulse design.

An alternative approach to derive a novel pulse shape from the sech/tanh pulse is to preserve the property of an elliptic pulse trajectory, but to abandon compliance with offset-independent adiabaticity, as was undertaken recently [14] using the numerically optimized modulation procedure (NOM) [15]. NOM optimizes the velocity of the effective field vector along the elliptic path by avoiding dropping of the adiabaticity parameter below a specified minimum value at any time during the pulse under allowance for variations in transition frequency and peak RF amplitude. Thus, in contrast to the principle of offset-independent adiabaticity, insensitivity to spatial RF inhomogeneity is actively designed. A further advantage of the NOM procedure is the feasibility of a trade-off between pulse performance parameters which was used to determine a pulse, tuned to 8 kHz bandwidth and 9 ms length, operating at possibly low peak RF amplitude. The optimized pulse has in comparison to the new pulse presented herein indeed a 11% lower peak RF amplitude, a 2% lower pulse energy, but performs significantly less selective, because of a transition region of twice the width [14].

In principle, the NOM procedure could be applied to the original constant adiabaticity pulse, i.e., for optimization of the velocity profile along the pulse trajectory made out of an infinite frequency sweep at constant RF amplitude. The drawbacks of the original constant adiabaticity pulse, high pulse energy and low selectivity, however, originate from that specific pulse trajectory and may experience only minor revision by NOM.

5. Conclusion

The principle of constant adiabaticity, enabling optimum adiabatic following of an individual isochromat, can be beneficial for broadband applications. In combination with the principle of offset-independent adiabaticity, enforcing a flat, localized power spectral density, an efficient selective adiabatic inversion pulse is obtained. Both principles concern desired global properties of the pulse to be obeyed at any instant throughout the total adiabatic transfer and are consequently expressed in differential form. In contrast, the most common approach to pulse design is to detail the desired pulse properties locally for any time point by stating explicitly the functional form of either the amplitude or the frequency modulation, or of either the trajectory of the effective field or the rate upon it [5,6,10,11,14,15]. In a sense, the design of the new adiabatic pulse is more closely related to the discovery of the well-known sech/tanh adiabatic pulse. The sech/tanh shape was anticipated because it allows for an analytical solution of the Schrödinger equation which in turn suggested its application for selective population inversion. In comparison with the sech/tanh pulse, the new adiabatic pulse achieves selective inversion with significantly reduced peak RF amplitude, and, thus, at largely relaxed hardware demands. It is particularly useful when spatial inhomogeneity of the RF amplitude across the sample volume is of lesser concern.

Acknowledgment

This work was supported in part by the Alexander von Humboldt-Foundation.

References

[1] C.E. Hughes, R. Kemp-Harper, S. Wimperis, NMR excitation of quadrupolar order using adiabatic demagnetization in the rotating frame, J. Chem. Phys. 108 (1998) 876–889.
[2] S. Hediger, B.H. Meier, R.R. Ernst, Adiabatic passage Hartmann-Hahn cross polarization in NMR under magic angle sample spinning, Chem. Phys. Lett. 240 (1995) 449–456.
[3] W. Peti, C. Griesinger, W. Bermel, Adiabatic TOCSY for C,C and H,H J-transfer, J. Biomol. NMR 18 (2000) 199–205.
[4] V.J. Basus, P.D. Ellis, H.D.W. Hill, J.S. Waugh, Utilization of chirp frequency modulation with 180°-phase modulation for heteronuclear spin decoupling, J. Magn. Reson. 35 (1979) 19–37.
[5] R. Freeman, E. Kupce, Decoupling: theory and practice I, NMR Biomed. 10 (1997) 372–380.
[6] M. Garwood, L. DelaBarre, The return of the frequency sweep: designing adiabatic pulses for contemporary NMR, J. Magn. Reson. 153 (2001) 155–177.
[7] A. Messiah, Quantum Mechanics, North Holland Press, Amsterdam, 1963.
[8] J. Baum, R. Tycko, A. Pines, Broadband and adiabatic inversion of a two-level system by phase-modulated pulses, Phys. Rev. A 32 (1985) 3435–3447.
[9] M.S. Silver, R.I. Joseph, D.I. Hoult, Selective spin inversion in nuclear magnetic resonance and coherent optics through an exact solution of the Bloch–Riccati equation, Phys. Rev. A 31 (1985) 2753–2755.

[10] E. Kupce, R. Freeman, Optimized adiabatic pulses for wideband spin inversion, J. Magn. Reson. A 118 (1996) 299–303.
[11] A. Tannus, M. Garwood, Improved performance of frequency-swept pulses using offset-independent adiabaticity, J. Magn. Reson. A 120 (1996) 133–137.
[12] Samples of the normalized amplitude and frequency modulations of the new adiabatic inversion pulse as functions of time may be downloaded from the internet web www.berlin.ptb.de/8/81/811/Download/_indexe.html.
[13] S.A. Smith, T.O. Levante, B.H. Meier, R.R. Ernst, Computer simulations in magnetic resonance. An object oriented programming approach, J. Magn. Reson. A 106 (1994) 75–89.
[14] D. Rosenfeld, S.L. Panfil, Y. Zur, Design of selective adiabatic inversion pulses using the adiabatic condition, J. Magn. Reson. 129 (1997) 115–124.
[15] K. Ugurbil, M. Garwood, A.L. Rath, Optimization of modulation functions to improve insensitivity of adiabatic pulses to variations in B_1 magnitude, J. Magn. Reson. 80 (1988) 448–469.